JOURNAL OF SPACECRAFT AND ROCKETS
Vol. 33, No. 5, September–October 1996

Comparison of Catalytic Wall Conditions for Hypersonic Flow

M. Barbato*
Centre for Advanced Studies, Research and Development in Sardinia, Cagliari 09123, Italy
D. Giordano† and J. Muylaert‡
European Space Agency, 2200 AG Noordwijk, The Netherlands
and
C. Bruno§
Università di Roma I, Rome 00184, Italy

The effects of several catalytic boundary conditions implemented in a hypersonic flow solver are analyzed for a sphere/cone geometry representative of a re-entry body. The three-dimensional Navier–Stokes equations solver uses a five-chemical-species model. The simulated surface is silica, representative of coatings for thermal protection systems. The range of wall temperatures explored is 300–1500 K, and fully catalytic, local-equilibrium, noncatalytic, and finite-rate catalysis boundary conditions are applied and discussed. For finite-rate catalysis a recent model for simultaneous recombination of O and N atoms, including NO formation, is used. A comparison of all the boundary conditions implemented with results from fit-based finite-rate catalysis boundary conditions is made at surface temperatures of 1200 and 1500 K. Numerical simulations results are compared and discussed, and conclusions about which boundary conditions are best in each case are drawn.

Nomenclature

A = atom
$\mathcal{D}_{ij}$ = binary diffusion coefficient, m^2/s
$\mathcal{D}_{mj}$ = multidiffusion coefficient, m^2/s
$\boldsymbol{j}_i$ = species-i diffusion flux vector, kg/(s m^2)
j_{iw} = component of $\boldsymbol{j}_i$ perpendicular to the body surface
$K_{w,i}$ = catalytic reaction rate constant (catalyticity), m/s
k = Boltzmann constant, 1.38066 J/K
L = body length, m
M = gas mixture molecular weight
Ma = Mach number
M_i = species-i molecular weight
m = reaction order
m_i = molecular mass of species i, kg
n = time step
n_i = particle-i number density, particle/m^3
p = pressure, Pa
p_i = partial pressure, Pa
$\dot{q}$ = heat flux, W/m^2
T = temperature, K
t = time, s
$\boldsymbol{V}$ = flow velocity vector, m/s
v = diffusion velocity component, m/s
v_i = species-i diffusion velocity component, m/s
X_i = molar fraction of chemical species i
Y_i = mass fraction of chemical species i
y = coordinate perpendicular to the body surface, m
Z = particle flux, particles/m^2
α = angle of incidence, deg
β = chemical energy accommodation factor
γ = recombination coefficient
Δy = distance between wall and first cell center, m
θ = surface coverage
ρ = mass density, kg/m^3

Subscripts

A = coordinate in the computational grid system
a = atom
d = diffusive
g = grid node nearest to the wall
rec = recombined
T = total
t = translational
v = vibrational
w = wall node; wall
∞ = freestream condition

Superscripts

n = time step
$*$ = adsorbed atom

Received May 8, 1995; revision received May 8, 1996; accepted for publication May 9, 1996.

*Research Engineer, Via Nazario Sauro 10. Member AIAA.
†Senior Researcher, P.O. Box 299, European Space Research and Technology Centre. Member AIAA.
‡Head of Aerothermodynamics Section, P.O. Box 299, European Space Research and Technology Centre. Member AIAA.
§Associate Professor, Dipartimento di Meccanica e Aeronautica, Via Eudossiana 18. Member AIAA.

Introduction

TO numerically simulate hypersonic flows, surface catalytic activity has always been a crucial item. The importance of these effects on a vehicle re-entering the atmosphere was pointed out theoretically in the late 1950s,[1] and since that time ground tests[2,3] and flight experiments[4] have demonstrated the large influence this phenomenon can have on surface heat transfer. In fact, during a re-entry in the atmosphere, part of the N and O atoms produced in the shock layer may reach the body surface and adsorb and/or react with other already adsorbed atoms, leaving the recombination energy at the surface. This diffusive contribution increases substantially the heat flux entering the surface. These gas–wall interactions, called heterogeneous recombinations, are typically very efficient, and their rate depends on the surface capability to enhance recombinations due to a more favorable energy balance (surface catalytic activity). Because of the significance of heterogeneous catalysis during re-entry, the Space Shuttle and future reusable thermal protection system (TPS) coatings, besides mechanical and thermal characteristics, must ensure very low catalytic activity, to reduce as much as possible the additional diffusive heat flux entering the body.

Looking at this problem, numerical simulation of heterogeneous-catalysis–hypersonic-flow coupling is clearly an outstanding and challenging task. In fact, the finite-rate catalytic activity of TPS surfaces depends on surface material, wall temperature,

gas characteristics (e.g. composition, pressure, temperature), and flow conditions. Accordingly, in numerical simulations often two extreme, and simple, boundary conditions (BC) have been used: noncatalytic wall (NCW) and local-equilibrium wall (LEW). More sophisticated BC are today more diffused, and finite-rate catalytic activity is modeled using fits[2] or correlations[5] coming from experimental data, or even using more fundamental models.[6,7]

In this work the effects of different catalytic BC on the numerical simulation of a hypersonic flow over a blunt body are investigated. The BC models implemented inside the numerical code TINA[8] are fully catalytic wall (FCW), LEW, noncatalytic wall, and finite-rate catalysis (FRC). The focus is on observing the predictions of these different models on varying the temperature from 300 up to 1500 K of silica (SiO_2) surfaces. Silica has been chosen because of its catalytic behavior, which represents well that of reaction-cured glass coatings[9] designed for the Space Shuttle TPS. Results of numerical simulations are compared and discussed, and conclusions about the most suitable boundary condition model to use in each case are drawn.

Problem Definition

The body shape investigated is a blunt cone with overall length 40 cm, nose radius 3.5 cm, and half cone angle 4.6 deg, a scaled model of the ELECTRE re-entry capsule[10] (Fig. 1). In the computational grid, the stagnation-point location for $\alpha = 0.0$ is $x_A = y_A = 0.0$. The freestream conditions are those specified in the Fourth European High-Velocity Database Workshop[11] held at the European Space Agency-European Space Research and Technology Center (ESA-ESTEC), Noordwijk, The Netherlands. These conditions are representative of the test chamber conditions of the F4 arc-jet wind tunnel located at ONERA, France. The freestream conditions (Table 1) show large differences between translational and vibrational temperatures (strong vibrational excitation in the freestream) and that O_2 is almost completely dissociated.

The numerical simulations presented in this work were performed with the code TINA[8] (thermochemical implicit nonequilibrium algorithm) developed by Netterfield following the work of Gnoffo.[12] TINA is a three-dimensional Navier–Stokes equation solver based on a finite-volume formulation, where the inviscid terms are expressed following the approximate Riemann solver of Roe.[13] A second-order-accurate scheme is achieved using the symmetric TVD flux limiters proposed by Yee.[14] The viscous fluxes

Table 1 Inflow conditions (ONERA-F4 test chamber conditions)

U_∞	5616.5 m/s
ρ_∞	6.9014×10^{-3} kg/m^3
L	0.4 m
T_∞	299.8 K
$T_{v\infty}$	5655.0 K
Ma	12.8
Y_{N_2}	0.7732
Y_N	0.0019
Y_{O_2}	0.0039
Y_O	0.2151
Y_{NO}	0.0059

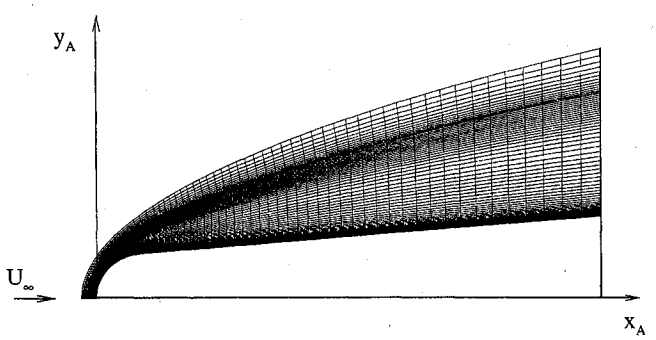

Fig. 1 ELECTRE geometry and grid used for the numerical tests: spherical nose radius, 0.035 m; half cone angle, 4.6 deg; overall length, 0.4 m; and grid points, 80 × 86.

are modeled following a thin-layer approximation, which neglects all viscous gradients except those in the direction normal to a solid surface. The steady-state solution is reached marching in time by means of a Gauss–Seidel relaxation technique.

Blottner's fits[15] describe single-species viscosities, and the mixture viscosity is calculated by Wilke's mixture rule.[16] Species thermal conductivities are obtained from the Eucken formula and polynomial fits for specific heats.[17] The mixture conductivity is calculated using the Wilke's rule. Binary diffusion coefficients are calculated from constant Schmidt numbers assumed for each species ($Sc = 0.5$). The multidiffusion coefficients are calculated using the formula found in Ref. 18.

Air chemistry is modeled according to Dunn and Kang[19]; a modified Arrhenius expression is used for the forward and backward rate coefficients. A two-temperature model[20] assumes a translational–rotational temperature T, and a single vibrational temperature T_v describing all the vibrational and electronic temperatures. The vibrational–translational relaxation is based on the Landau–Teller theory,[21] and the relaxation time is that of Millikan and White,[22] with the Park correction[20] for temperatures >8000 K.

The effect of vibrational energy on forward dissociation rates is taken into account by using the averaged temperature model proposed by Park[20] ($T_q = T^b T_v^{1-b}$; $b = 0.5$). A nonpreferential dissociation model evaluates the amount of dissociation energy removed from the vibrational energy.

Surface Boundary Conditions

At the surface we assume nonslip conditions and a nonablative, impermeable, isothermal wall. As BC for the vibrational temperature we assume local thermal equilibrium, i.e., $(T_v)_w = T_w$ everywhere. Four catalytic BC are examined: FCW, LEW, FRC, and NCW. The wall temperatures investigated run from 300 to 1500 K.

Finite-Rate Catalysis

To introduce the key quantities for this BC we consider a gas mixture of atoms A and molecules A_2; following Goulard,[1] the atoms source term reads

$$\dot{w}_a = K_{w,a}(\rho_w Y_{wa})^m \tag{1}$$

where $K_{w,a}$ is defined as the constant factor by which the gas phase density of atoms at the surface must be multiplied to obtain the surface rate of conversion of atoms into molecules per unit area and unit time[23]:

$$Z_{a,\mathrm{rec}} = K_{w,a} n_a \tag{2}$$

Together with $K_{w,a}$, the catalytic behavior of a gas–surface system may be expressed in terms of the recombination probability γ defined as

$$\gamma = \frac{\text{flux of atoms recombined on the surface}}{\text{flux of atoms impinging on the surface}} = \frac{Z_{a,\mathrm{rec}}}{Z_a} \tag{3}$$

From Eqs. (2) and (3) and assuming the surface planar,[21]

$$Z_a = \frac{n_a kT}{\sqrt{2\pi m_a kT}} \tag{4}$$

the Hertz–Knudsen relation[24] is derived:

$$K_{w,a} = \gamma\sqrt{kT_w/2\pi m_a} \tag{5}$$

Equation (5) is the same expression obtained by Scott[23] for no-slip condition and a velocity distribution function without perturbation terms. From Eq. (5), γ may be seen as the ratio between the velocity associated to the flux of recombining atoms, and their kinetic velocity (at the wall temperature). Once either $K_{w,a}$ or γ is known, the surface chemical source term can be expressed using Eqs. (5) and/or (1).

Experimental fits of γ for separate N and O atoms recombinations on high-temperature reusable system insulation (HRSI) surfaces were obtained[2] from calorimetric measurements:

$$\gamma' = Be^{C/T_W} \tag{6}$$

In Eq. (6) γ' is the energy-transfer catalytic recombination coefficient. Since $\gamma' = \beta\gamma$, the two recombination coefficients γ and γ' have the same value only when the residence time for recombined molecules is long enough to complete the transfer of all recombination energy to the wall, i.e., when $\beta = 1$ (Ref. 25).

Noncatalytic Wall

This is an extreme condition: the wall is considered to be absolutely indifferent to kinetics. There is no species depletion or production at the wall, $\dot{w}_{wa} = 0$, and, from Eq. (1), $K_{w,a} = 0$. A noncatalytic wall is defined as a surface with zero catalyticity and zero γ for each species.

Fully Catalytic Wall

Under the FCW assumption, the wall is an infinitely efficient catalyst, i.e., $\gamma = 1$ and therefore $X_{wa} = 0$ (complete recombination). For air, only O_2, N_2, and NO may exist on the surface. From Eq. (1), and since for steady state $-j_{aw} = \dot{w}_{aw}$, $K_{w,a}$ becomes infinite.

This BC is not influenced by heterogeneous kinetics: recombination is controlled by the atom diffusion velocity. Therefore, the fully catalytic condition is, in fact, a diffusion-dominated catalysis condition.

Local Equilibrium

LEW (often erroneously referred to as FCW) consists in assuming the gas composition at the wall equal to that at local equilibrium. For $T_w < 2000$ K this condition is well represented by molar fractions $X_{O_2} = 0.21$ and $X_{N_2} = 0.79$, i.e., $X_N = X_O = X_{NO} = 0$. Clearly this BC is stronger than the previous one: besides complete independence from the wall material behavior, LEW also forces the atoms' flux towards the wall. Therefore, while FCW atom recombination is driven by the flux of atoms reaching the wall, LEW instead itself drives the atom fluxes. Over a broad range of T_w FCW and LEW may, therefore, produce different results.

Finite-Rate Catalysis Model

The FRC model CORICO[7] is used in this study. This model calculates three independent recombination coefficients (γ_N, γ_O, and γ_{NO}) accounting for N_2, O_2, and NO surface formation. The surface is assumed to be pure silica, simulating RCG catalytic behavior.[9] Besides simultaneous adsorption of N and O atoms, the model allows also for the presence of OH radicals strongly bonded with the silica lattice, and coming from H_2O adsorption. These adsorbed radicals reduce the number of sites available to O and N atoms. This phenomenon has been taken into account because, due to the strong Si–OH bond, when silica is exposed to a wet atmosphere, these radicals tend to remain bonded on the surface even at $T = 1200$ K (Ref. 26).

The heterogeneous kinetics mechanisms accounted for by CORICO is[7]

$$A + * \rightarrow A^* \qquad \text{(adsorption)}$$

$$A + A^* \rightarrow A_2 + * \qquad \text{(Eley–Rideal recombination)}$$

$$A^* + A^* \rightarrow A_2 + 2* \qquad \text{(Langmuir–Hinshelwood recombination)}$$

$$A^* \rightarrow A + * \qquad \text{(thermal desorption)}$$

where $*$ represents an adsorption surface site, i.e., a surface location where an N or O atom can be chemically bonded. As can be seen, two surface reaction mechanisms are modeled: Eley–Rideal (ER), i.e., reaction between gas atom and adsorbed atom (adatom), and Langmuir–Hinshelwood (LH), i.e., reaction between two adatoms. The recombination coefficients are calculated through a balance of adsorbed, recombined, and thermally desorbed atoms and are functions of wall temperature and gas composition (i.e., O and N partial pressures at the wall). The model has been validated[7] for O–O_2 and N–N_2 mixtures flows, using Scott's results[2] and Berkut et al.'s results,[3] showing good agreement. The use of models like the one utilized here overcomes one of the limitations of experimentally derived fit-based FRC: the validity in a usually narrow temperature range. In fact, CORICO's applicability range goes from ambient temperature up to the silica melting point without need of risky extrapolation. In contrast with correlation-based FRC derived from flight data, e.g., the one of Ref. 5, these FRC models offer the capability to numerically simulate flow conditions not yet experimentally tested.

Boundary Condition Implementation

To write the diffusion velocity boundary conditions, we adopt a simplified expression[27] derived from the Stefan–Maxwell equations,[28] assuming that all but the ith species move with the same velocity v; therefore, the chemical species fluxes entering the surface are

$$\rho_i v_i = -\rho \mathcal{D}_{mi} \frac{\partial X_i}{\partial y}, \qquad i = 1, \ldots, 5 \tag{7}$$

where the multidiffusion coefficient reads

$$\mathcal{D}_{mi} = \frac{M_i}{M} \frac{1 - Y_i}{\sum_{j=1,\, j\neq i}^{5} X_j / \mathcal{D}_{ij}}, \qquad i, j = 1, \ldots, 5 \tag{8}$$

These simplified expressions do not respect the constraint

$$\sum_{i=1}^{5} \rho_i v_i = 0 \tag{9}$$

To remove this inconsistency, we assume a corrected diffusion velocity[27]:

$$v_i' = v_i + v_c, \qquad i = 1, \ldots, 5 \tag{10}$$

where v_c is defined imposing the constraint shown in Eq. (9). Therefore, Eq. (7) is replaced by

$$\rho_i v_i' = -\rho \mathcal{D}_{mi} \frac{\partial X_i}{\partial y} + Y_i \rho \sum_{j=1}^{5} \mathcal{D}_{mj} \frac{\partial X_j}{\partial y}, \qquad i = 1, \ldots, 5 \tag{11}$$

The analytical wall boundary condition for the five chemical species is obtained by imposing steady-state mass species conservation at the wall[29]:

$$(\dot{w}_i)_w = -(\rho_i v_i')_w, \qquad i = 1, \ldots, 5 \tag{12}$$

which by Eq. (11) becomes

$$(\dot{w}_i)_w = \left(\rho \mathcal{D}_{mi} \frac{\partial X_i}{\partial y}\right)_w - Y_{iw} \rho_w \sum_{j=1}^{5} \left(\mathcal{D}_{mj} \frac{\partial X_j}{\partial y}\right)_w$$

$$i = 1, \ldots, 5 \tag{13}$$

The numerical solution of the flowfield requires the molar fractions at the wall; after a first-order finite difference discretization of Eq. (13), we have

$$X_{iw}^n = X_{ig}^n - \left(\frac{\Delta y}{\rho \mathcal{D}_{mi}}\right)_w^n \left[\dot{w}_{iw}^n + Y_{iw}^n \rho_w^n \sum_{j=1}^{5} \left(\mathcal{D}_{mj} \frac{X_{ig} - X_{iw}}{\Delta y}\right)^n\right]$$

$$i = 1, \ldots, 5 \tag{14}$$

This set of BC was applied to each wall grid node.

For the NCW case, Eq. (14) becomes

$$X_{iw}^n = X_{ig}^n - \left(\frac{\Delta y}{\rho \mathcal{D}_{mi}}\right)_w^n \left[Y_{iw}^n \rho_w^n \sum_{j=1}^{5} \left(\mathcal{D}_{mj} \frac{X_{ig} - X_{iw}}{\Delta y}\right)^n\right]$$

$$i = 1, \ldots, 5 \tag{15}$$

because $\dot{w}_i = 0$ for each species i. For the FCW case, the BC are obtained using Eq. (14), where $\dot{w}_{iw}^n$ are calculated assuming $\gamma = 1$ for all species except NO, for which we assume $\dot{w}_{NOw}^n = 0$. The LEW BC become

$$X_{iw}^n = \bar{X}_i, \qquad i = 1, \ldots, 5 \tag{16}$$

where $\bar{X}_i$ is the equilibrium value of species i at $T = T_w$ and $p = p_w$.

For the FRC case, Eq. (14) is implicit (all the quantities are evaluated at the time n). Therefore, wall chemical source terms were quasilinearized:

$$\dot{w}_{iw}^n \approx \dot{w}_{iw}^{n-1} + \sum_{j=1}^{ns} \left(\frac{\partial \dot{w}_{iw}}{\partial X_{jw}} \right)^{n-1} \left(X_{jw}^n - X_{jw}^{n-1} \right) \tag{17}$$

and the correction, i.e., the second term inside the square brackets, is calculated at the time $n - 1$. The wall molar fractions X_{iw}^n for the five species at the time n were obtained from Eqs. (14) and (17) using Eqs. (1) and (5) to calculate $\dot{w}_{iw}$.

Results

The results presented in the next subsections refer to test cases with the same freestream conditions of Table 1.

T_w = 300 K

Noncatalytic wall behavior is expected under these conditions[7] ($\gamma \sim 10^{-4}$, as shown by Fig. 2), because the temperature is too low to activate recombination and the OH surface coverage is high (Fig. 3), leaving few free sites for O and N adsorption. Accordingly, the curves relative to the FRC and NCW models coincide in Figs. 4 and 5, where the X_i and T plots on the stagnation line are shown. Large differences exist between these results and those of the FCW and LEW cases. An interesting unexpected behavior is that of X_{NO}: for the latter two cases this molar fraction has a maximum

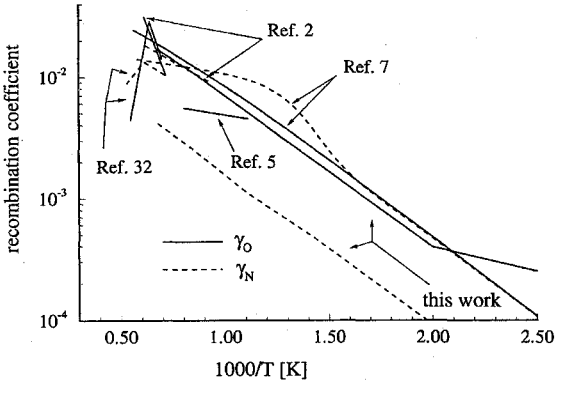

Fig. 2 Oxygen and nitrogen recombination coefficients vs inverse temperature.

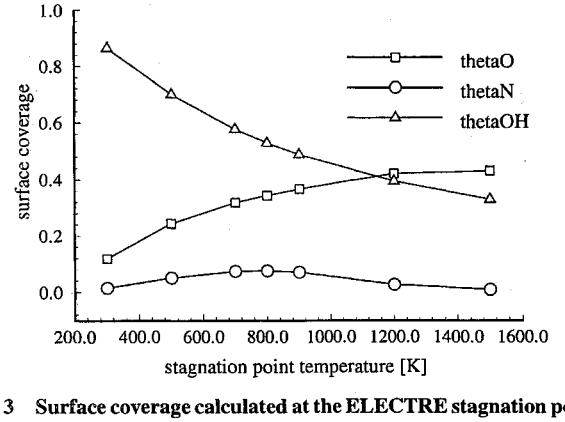

Fig. 3 Surface coverage calculated at the ELECTRE stagnation point.

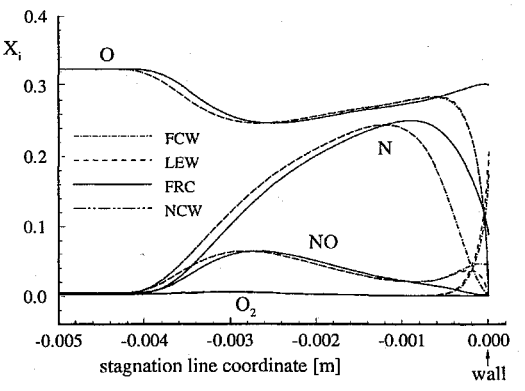

Fig. 4 Stagnation-line molar fractions (T_w = 300 K).

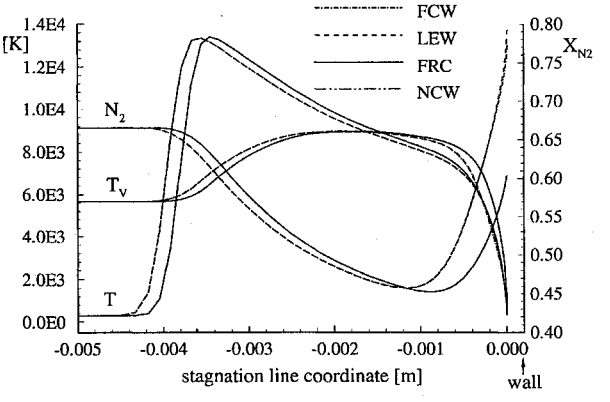

Fig. 5 Stagnation-line temperatures and N_2 molar fraction (T_w = 300 K).

near the surface. This NO production is due to the gas phase mechanism

$$O_2 + N \longrightarrow NO + O + 32.4 \text{ kcal/mole}$$

$$N_2 + O + 76.4 \text{ kcal/mole} \longrightarrow NO + N$$

which is very efficient because of the very low activation energy of the first reaction and the large O_2 and N_2 concentrations close to the surface. On approaching the wall, X_{NO} behaves differently depending on the BC used: for the LEW case, the NO molar fraction is forced to go to zero at wall; consequently a steep X_{NO} gradient is formed. On the contrary, for the FCW case, going toward the wall, the molar fraction changes little; it has a smaller gradient and a nonzero value at the surface. Because of the near absence of O_2 near to the wall, both FRC and NCW cases show smoother NO profiles when moving toward the wall.

Another difference is the shock standoff distance, which is slightly larger when FCW and LEW BC are used: although the mixture density after the shock is higher for these cases, the huge number of molecules produced by the wall seems to push back the shock. Moreover, with these BC the flux of recombined molecules (in local thermal equilibrium) leaves the wall and cools the hotter internal degrees of freedom of the gas near the surface, lowering T_v and leading to a thicker thermal boundary layer for T_v than in the cases of FRC, with fewer wall-recombined molecules, and NCW, with no wall-recombined molecules (Fig. 5). This has consequences for the vibrational contributions ($\dot{q}_v$) to the total surface heat flux ($\dot{q}_T$). In fact, Fig. 6 shows $\dot{q}_{v\,FCW}$ and $\dot{q}_{v\,LEW}$ are everywhere lower than $\dot{q}_{v\,FRC}$ and $\dot{q}_{v\,NCW}$. This affects, to a smaller extent, T also, as shown by Fig. 7, where the translational contributions ($\dot{q}_t$) are shown.

The weak catalytic activity of silica at $T_w = 300$ K is shown by the substantial difference between the diffusive contributions $\dot{q}_{d\,FCW}$, $\dot{q}_{d\,LEW}$, and $\dot{q}_{d\,FRC}$ (Fig. 8) and by the fact that the ratio $\dot{q}_{T\,FRC}/\dot{q}_{T\,NCW}$ is almost equal to one everywhere along the body (Fig. 9). The results obtained using FCW (and LEW) overpredict $\dot{q}_T$ by as much as 55%. $\dot{q}_{T\,FCW}$ is slightly smaller than $\dot{q}_{T\,LEW}$ (1.6%) because, for the FCW case, $X_{NOw} \neq 0$ and the atoms forming NO in

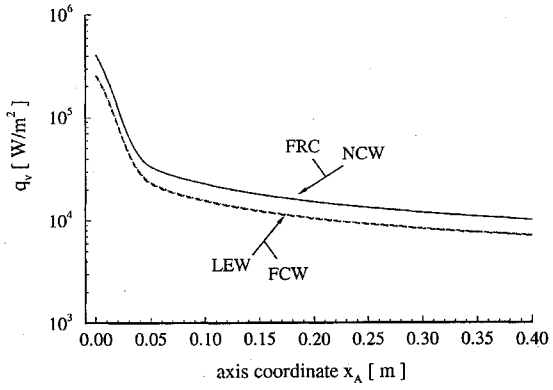

Fig. 6 Comparison among vibrational heat fluxes (T_w = 300 K).

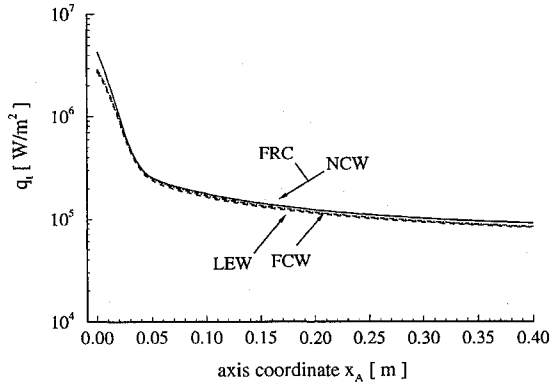

Fig. 7 Comparison among translational heat fluxes (T_w = 300 K).

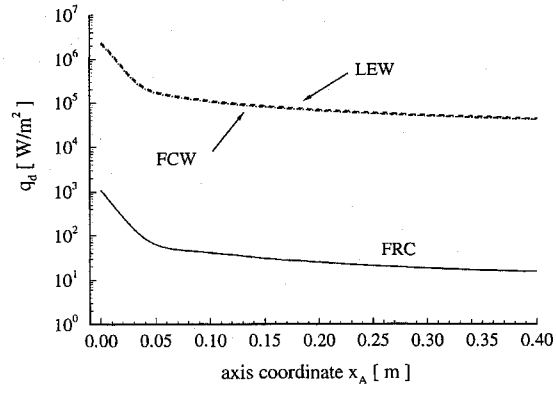

Fig. 8 Comparison among diffusive heat fluxes (T_w = 300 K).

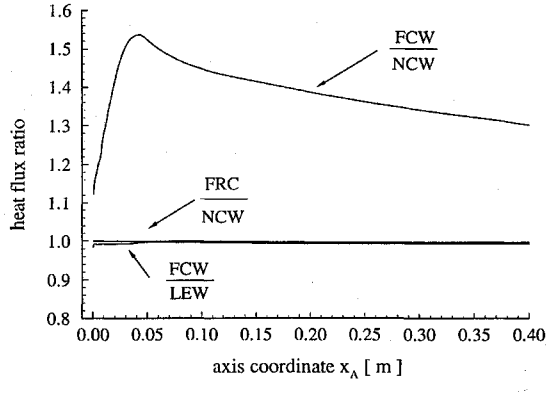

Fig. 9 Total heat flux ratios (T_w = 300 K).

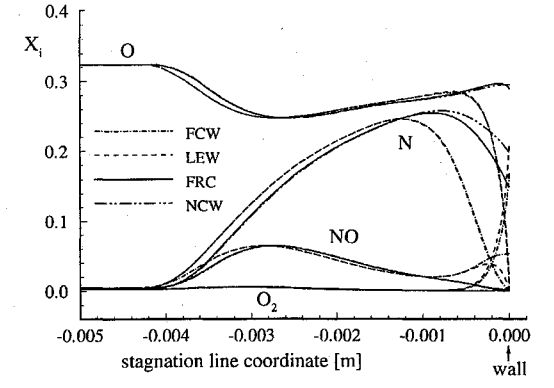

Fig. 10 Stagnation line molar fractions (T_w = 800 K).

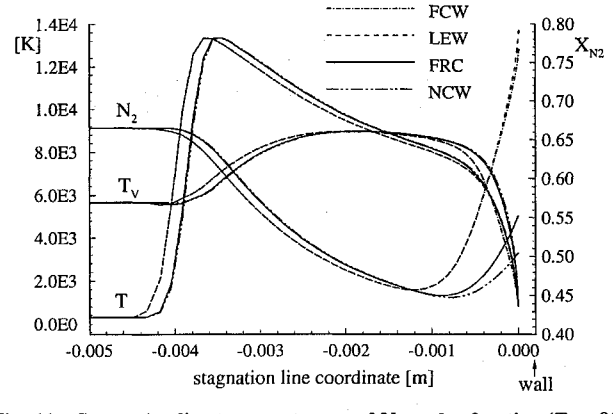

Fig. 11 Stagnation line temperatures and N_2 molar fraction (T_w = 800 K).

the gas phase are no longer available for a possible heterogeneous recombination. Therefore, the main conclusion for the $T_w = 300$ K case is that a silica surface behaves decidedly as noncatalytic, and that the NCW is a good approximation at this temperature. The FCW and LEW overpredict $\dot{q}_T$ and also misrepresent molar fractions near the surface, therefore misrepresenting the density.

T_w = 800 K

Compared to the $T_w = 300$ K case, the wall catalytic activity increases, as shown by the stagnation-line molar fraction plots of Figs. 10 and 11: the FRC BC predict larger O, N consumption and larger N_2, O_2 formation. The higher atom recombination rate is due to the activation of heterogeneous catalysis processes (starting with the ER mechanism) and to the lower OH surface coverage (see Fig. 3). This increased catalytic activity leads also to wall production of NO, as displayed by Fig. 12, where $X_{NO,w}$ for the FRC case is small but larger than in the NCW case. This fact can be important because surface recombination forming NO is less exothermic than N_2 and O_2 recombination.[30] Thus, a model allowing for NO recombination predicts a diffusive thermal flux lower than that predicted by a model allowing for N_2 and O_2 recombination only.

The increased catalytic activity implies a larger $\dot{q}_d$ than in the lower-temperature case. In fact, for $T_w = 800$ K, $\dot{q}_{d\,\mathrm{FRC}}$ is closer to $\dot{q}_{d\,\mathrm{FCW}}$ and $\dot{q}_{d\,\mathrm{LEW}}$: the average difference is less than one order of magnitude, compared with three orders of magnitude for $T_w = 300$ K (Figs. 8 and 13). A comparison among the $\dot{q}_T$ is shown in Fig. 14. At this wall temperature the FRC/NCW ratio is greater than one all along the body, and on the spherical part of ELECTRE, $\dot{q}_{T\,\mathrm{FRC}}$ is up to 13% higher than $\dot{q}_{T\,\mathrm{NCW}}$. Besides, $\dot{q}_{T\,\mathrm{FCW}}$ is up to 53% higher than $\dot{q}_{T\,\mathrm{FRC}}$, and slightly smaller than $\dot{q}_{T\,\mathrm{LEW}}$ (1%).

At $T_w = 800$ K we can conclude that the results obtained using FRC and NCW BC differ substantially because catalysis is activated. Therefore, if the FCW and LEW models are too extreme as approximations (too much recombination, overestimated thermal load, and poor estimate of wall molar fractions), the NCW model is also extreme (no recombination allowed for, underestimated thermal load, and poorly estimated wall molar fractions and density). At this T_w, assuming a FRC BC model is necessary.

T_w = 1200 K

At 1200-K wall temperature, the catalytic activity is still higher, and on the ELECTRE nose $\dot{q}_{T\,\mathrm{FRC}}$ is up to 39% higher than $\dot{q}_{T\,\mathrm{NCW}}$ (Fig. 15). The FCW BC overestimate $\dot{q}_T$ up to 45% with respect to FRC BC, suggesting that the former BC are unsuitable for a silica surface also at 1200 K, and that FRC BC are the most appropriate. At this temperature a further comparison has been performed with the FRC BC based on the Zoby et al.[5] correlation inferred from the STS-2 Space Shuttle flight data and referred to hereinafter as FRC-1. In this case the oxygen recombination coefficient is[5]

$$\gamma_O = 0.00941e^{-658.9/T_w}, \qquad 900 < T_w < 1250\,\mathrm{K} \qquad (18)$$

whereas for the nitrogen recombination coefficient we assume Scott's expression[2] (as done in Ref. 31)

$$\gamma_N = 0.0714e^{-2219/T_w}, \qquad 950 < T_w < 1670\,\mathrm{K} \qquad (19)$$

Comparison among the different FRC models shows that the maximum difference between $\dot{q}_{d\,\mathrm{FRC}}$ and $\dot{q}_{d\,\mathrm{FRC\text{-}1}}$ is about 30% (Fig. 16), but that between $\dot{q}_{T\,\mathrm{FRC}}$ and $\dot{q}_{T\,\mathrm{FRC\text{-}1}}$ is only 6.4%. This happens because the highest $\dot{q}_d$ corresponds to the lowest $\dot{q}_v$ and $\dot{q}_t$ (assuming

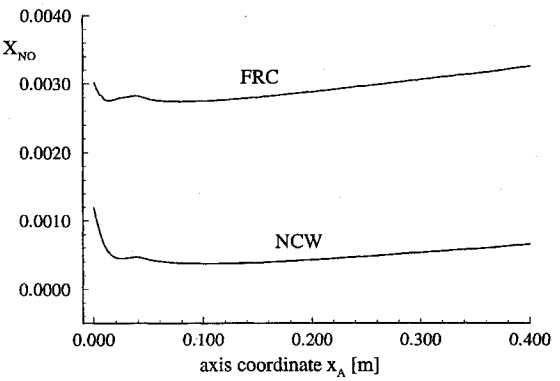

Fig. 12 NO molar fraction along the ELECTRE surface (T_w = 800 K).

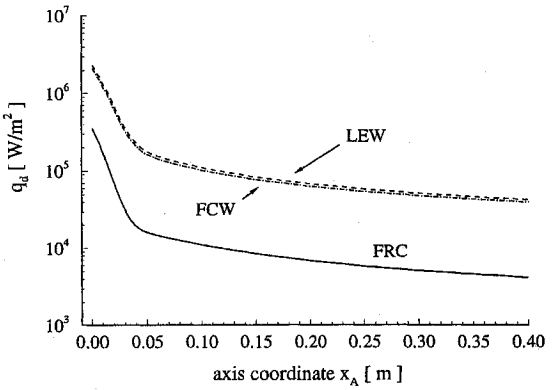

Fig. 13 Comparison among diffusive heat fluxes (T_w = 800 K).

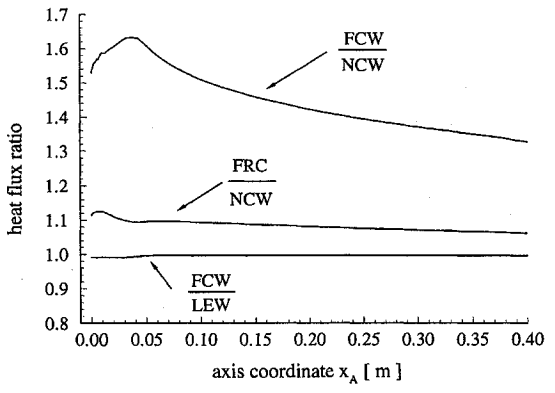

Fig. 14 Total heat flux ratios (T_w = 800 K).

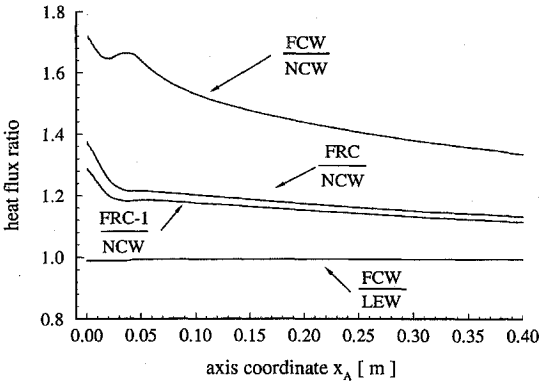

Fig. 15 Total heat flux ratios (T_w = 1200 K).

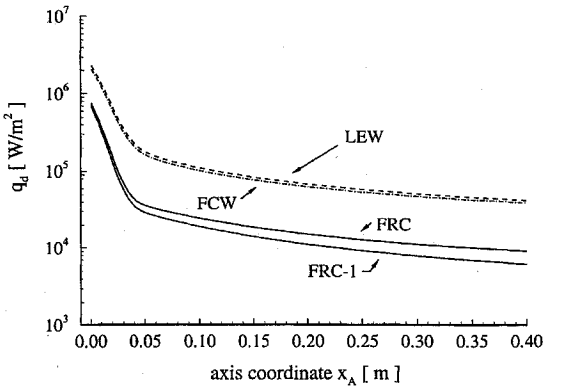

Fig. 16 Comparison among diffusive heat fluxes (T_w = 1200 K).

$\beta = 1$, higher recombination means lower vibrational and translational gas temperatures near the surface). At this temperature, the use of one of these two FRC models is recommended.

T_w = 1500 K

At $T_w = 1500$ K, three different FRC BC were compared: CORICO, Scott's fits,[2] and Kolodziej and Stewart's fits.[32] Hereinafter these models are referred as FRC, FRC-2, and FRC-3, respectively. The two last correlations are relative to the formation of only N_2 and only O_2 on HRSI. Scott's fits for the recombination coefficients[2] are

$$\gamma_N = 0.0714e^{-2219/T_w}, \qquad 950 < T_w < 1670\,\mathrm{K} \qquad (20)$$

$$\gamma_O = 16.0e^{-10271/T_w}, \qquad 1400 < T_w < 1650\,\mathrm{K} \qquad (21)$$

whereas those of Kolodziej and Stewart[32] are

$$\gamma_N = 0.061e^{-2480/T_w}, \qquad 1410 < T_w < 1640\,\mathrm{K} \qquad (22)$$

$$\gamma_O = 40.0e^{-11440/T_w}, \qquad 1435 < T_w < 1580\,\mathrm{K} \qquad (23)$$

Neither Scott nor Kolodziej and Stewart allow for the surface formation of NO, and their γ's were obtained from experiments using either pure N_2 or pure O_2. The recombination coefficients obtained using these models are in Fig. 2.

The thermal loads at 1500 K show that the $\dot{q}_d$ for the three FRC models are very close to each other (1–5% difference) with FRC-2 giving the largest values (Fig. 17). All three $\dot{q}_d$ are noticeably lower than those calculated using FCW and LEW. The differences existing among the $\dot{q}_T$ can be seen in Fig. 18: on the ELECTRE conical part $\dot{q}_{T\,\mathrm{FCW}}$ is 15% higher than $\dot{q}_{T\,\mathrm{FRC}}$, and that difference grows to 32% over the nose. Similarly, the difference between $\dot{q}_{T\,\mathrm{FCW}}$ and $\dot{q}_{T\,\mathrm{NCW}}$ is also large, ranging from a minimum of 40% to a maximum of 80%. To conclude, also at this wall temperature an FRC boundary condition should be implemented. The three models tested here behave similarly, and in fact, differences among $\dot{q}_{T\,\mathrm{FRC}}$, $\dot{q}_{T\,\mathrm{FRC\text{-}2}}$, and $\dot{q}_{T\,\mathrm{FRC\text{-}3}}$ are less than 2%.

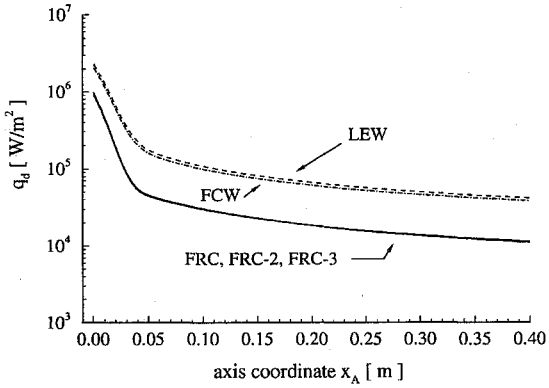

Fig. 17 Comparison among diffusive heat fluxes (T_w = 1500 K).

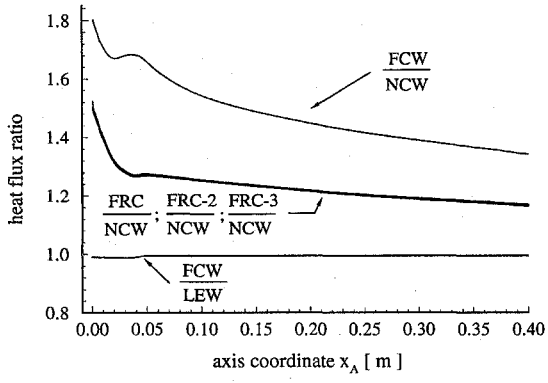

Fig. 18 Total heat flux ratios (T_w = 1500 K).

Thermal Load and Catalysis Effects

Thermal loads for T_w = 300–1500 K are shown in Figs. 19–22. These were predicted with FRC BC based on CORICO. From Fig. 19 we see that the translational heat flux decreases when the wall temperature increases (by going from 90 to 70% of $\dot{q}_T$), because the translational temperature gradient becomes weaker; the same happens to the vibrational contribution (Fig. 20), for which, moreover, the quenching action of freshly recombined molecules grows more effective with T_w in reducing the vibrational temperature gradient at the wall ($\dot{q}_v$ goes from 12 to 8% of $\dot{q}_T$). The diffusive contribution, displayed in Fig. 21, increases rapidly when T_w goes from 300 to 1500 K (from 0.02 to 20% of $\dot{q}_T$), on account of increasing catalytic activity (see Fig. 2). Figure 2 emphasizes also a difference between the recombination coefficients predicted by CORICO for pure species fluxes[7] (i.e., the experimental conditions of Refs. 2 and 3) and those calculated, in this work, in real flow conditions. The latter γ for ELECTRE are lower because there is competition between N and O atoms, not present when either O or N adsorption is allowed for (the presence of nitrogen atoms adsorbed at the surface reduces the recombination probability of O and vice versa). Furthermore, the catalytic formation of NO reduces the recombination probability of O and N. As noticed, these coupling effects cannot be taken into account using fit-based FRC BC. Concerning the total heat flux entering the body surface, Fig. 22 shows that in the spherical part $\dot{q}_T$ varies inversely as the wall temperature (strong dominance of conductive contributions), whereas in the cone part $\dot{q}_T$ grows with the wall temperature.

It is interesting to look at CORICO predictions to interpret the mechanisms of guiding N_2 and O_2 recombination. The driving mechanism of $N + N \rightarrow N_2$ at low T_w is the ER mechanism, because its activation energy is low (20 kJ/mole; see Ref. 7) At $T_w > 900$ K the LH mechanism becomes dominant,[7] as also shown in Fig. 3 by the surface-coverage decrease. (The LH mechanism is very effective in reducing coverage, because for each recombination two atoms leave the wall.) At higher temperatures, the N_2 recombination reaction is very rapid because both mechanisms are completely activated.

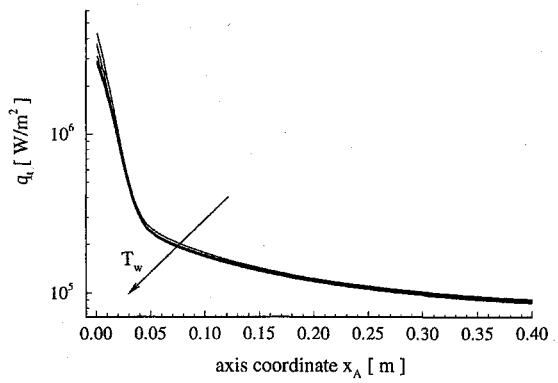

Fig. 19 Comparison among translational heat fluxes with wall temperature variation (T_w = 300, 500, 700, 900, 1200, and 1500 K).

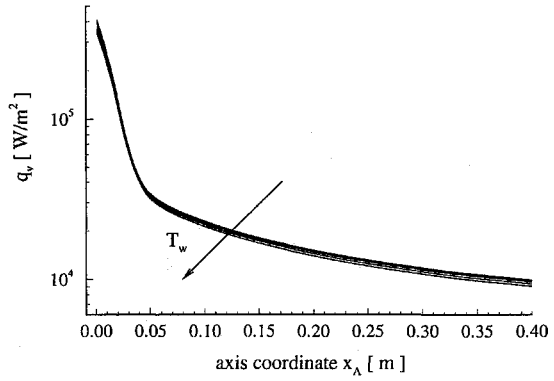

Fig. 20 Comparison among vibrational heat fluxes with wall temperature variation (T_w = 300, 500, 700, 900, 1200, and 1500 K).

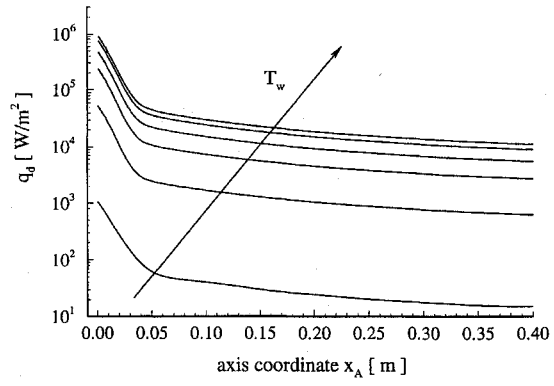

Fig. 21 Comparison among diffusive heat fluxes with wall temperature variation (T_w = 300, 500, 700, 900, 1200, and 1500 K).

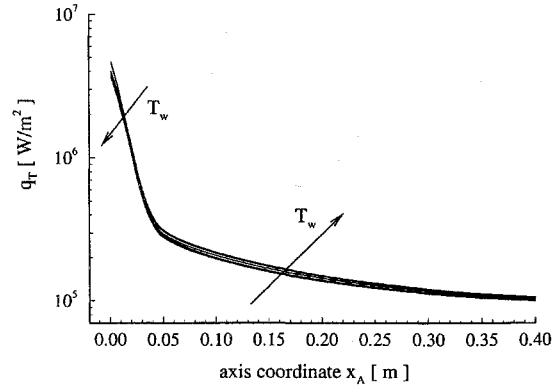

Fig. 22 Comparison among total heat fluxes with wall temperature variation (T_w = 300, 500, 700, 900, 1200, and 1500 K).

As for O_2, the catalytic mechanism driving $O + O \rightarrow O_2$ in the 500–1500-K range is the ER, because the LH has a large activation energy (501 kJ/mole; see Ref. 7) In fact, the slope of the O surface coverage above 1000 K changes slowly, since the ER mechanism is already fully activated whereas the LH is not. The ER mechanism dominates the recombination $N + O \rightarrow NO$ at all temperatures in the range examined[7]; in particular, the recombination $N_{gas} + O_{ads} \rightarrow NO$ is the most probable ($\theta_O > \theta_N$).

Based on these results, and by observing that molecules recombined by the ER mechanism should leave the wall in thermal non-equilibrium,[24] the assumption $\beta = 1$ appears weak at lower temperatures and reasonable only for N_2 formation at higher temperatures. In fact, the probability of desorption in local thermal equilibrium is much higher for LH than it is for ER. Therefore, retaining the assumption $\beta = 1$, we observe that when the wall temperature increases and notwithstanding the decrease of $\dot{q}_t$ and $\dot{q}_v$, in the conical part of the body the total heat flux becomes larger because of the large increase of $\dot{q}_d$ (see Fig. 22).

Conclusions

The FRC model applied to lower T_w (300 K) shows a surface with a practically noncatalytic behavior; for $T_w > 500$ K the surface shows moderate catalytic activity that increases with wall temperature. For the particular body shape and flow parameters explored in this work, we conclude that for a silica surface at low temperature ($T_w = 300-400$ K), noncatalytic BC are a reasonably good approximation, and a more complex model to simulate the wall heterogeneous chemistry effects is not needed. At higher temperatures ($T_w > 500$ K) and for the conditions considered in this work, we believe it necessary to use finite-rate catalytic BC to obtain realistic wall catalytic behavior, good estimates of the gas composition near the wall, and good evaluation of the wall thermal load.

Surface heat flux comparison between the CORICO model and other FRC models shows generally good agreement. An exception is the case $T_w = 1200$ K, where the FRC-1 model of Zoby et al. predicts a diffusive contribution 30% lower than that obtained with the FRC based on CORICO. This difference is balanced by the opposite difference in translational and vibrational contributions, leading to very similar total thermal loads. Compared to the other FRC models tested, CORICO covers a wider range of temperature ($T_w = 300$–1700 K) and calculates recombination coefficients allowing for realistic near-wall flow conditions.

In conclusion, care is needed when modeling the catalytic activity of silica-based TPS coatings in hypersonic flows. The use of FRC BC at the gas–wall interface is recommended. Fit-based models are not suitable when not just thermal loads, but also accurate near-wall gas composition (and density), are needed.

Acknowledgments

This work has been carried out with the financial help of the Sardinian Regional Government. The authors are grateful to the ESA-ESTEC Aerothermodynamics Section staff, and in particular to L. M. G: Walpot for his friendly help. Special thanks go to M. Netterfield.

References

[1]Goulard, R., "On Catalytic Recombination Rates in Hypersonic Stagnation Heat Transfer," *Jet Propulsion*, Vol. 39, Nov. 1958, pp. 737–745.

[2]Scott, C. D., "Catalytic Recombination of Nitrogen and Oxygen on High-Temperature Reusable Surface Insulation," *Aerothermodynamics and Planetary Entry*, edited by A. L. Crosbie, Vol. 77, Progress in Astronautics and Aeronautics, AIAA, New York, 1980, pp. 193–212.

[3]Berkut, V. D., Doroshenko, V. M., Zhdanok, S. A., Kovtun, V. V., Kudryavtsev, N. N., Novikov, S. S., and Sharovatiov, A. I., "Opredeleniye Veroyatnosti Geterogennoy Rekombinatsii Atomov na Nagretykh do Vysokikh Temperatur ($T_w = 1000$ K) Poverkhnostyakh Tvyordykh Tel, Obtekayemykh Dissotsiiro," Inst. Teplo-I Massoobmena Im. A. V. Lykova, Akad. Nauk BSSR, Preprint No. 8, Minsk, 1989, pp. 1–30.

[4]Stewart, D. A., Rakich, J. V., and Lanfranco, M. J., "Catalytic Surface Effects Experiment on the Space Shuttle," *Thermophysics of Atmospheric Entry*, edited by T. E. Horton, Vol. 82, Progress in Astronautics and Aeronautics, AIAA, New York, 1982, pp. 248–272.

[5]Zoby, E. V., Gupta, R. N., Jr., and Simmonds, A. L., "Temperature-Dependent Reaction-Rate Expression for Oxygen Recombination at Shuttle Entry Conditions," AIAA Paper 84-0224, Jan. 1984.

[6]Seward, W. A., and Jumper, E. J., "Model for Oxygen Recombination on Silicon-Dioxide Surfaces," *Journal of Thermophysics and Heat Transfer*, Vol. 5, No. 3, 1991, pp. 284–291.

[7]Nasuti, F., Barbato, M., and Bruno, C., "Material-Dependent Catalytic Recombination Modeling for Hypersonic Flows," *Journal of Thermophysics and Heat Transfer*, Vol. 10, No. 1, 1996, pp. 131–136; also AIAA Paper 93-2840, July 1993.

[8]Netterfield, M. P., "Validation of a Navier–Stokes Code for Thermochemical Non-Equilibrium Flows," AIAA Paper 92-2878, July 1992.

[9]Carleton, K. L., and Marinelli, W. J., "Spacecraft Thermal Energy Accomodation from Atomic Recombination," *Journal of Thermophysics and Heat Transfer*, Vol. 6, No. 4, 1992, pp. 650–655.

[10]Muylaert, J., Walpot, L., Häuser, J., Sagnier, P., Devezeaux, D., Papirnyk, O., and Lourme, D., "Standard Model Testing in the European High Enthalpy Facility F4 and Extrapolation to Flight," AIAA Paper 92-3905, July 1992.

[11]Sagnier, P., and Kordulla, W., "Synthesis of the Electre in F4 Test Case," *Proceedings of the 4th European High Velocity Database Workshop*, edited by J. A. Desideri, Wiley Interscience Europe, 1995, pp. 156–171.

[12]Gnoffo, P. A., "Upwind-Biased, Point Implicit Relaxation Strategies for Viscous, Hypersonic Flows," AIAA Paper 89-1772, June 1989.

[13]Roe, P. L., "Approximate Riemann Solvers, Parameters Vectors and Difference Schemes," *Journal of Computational Physics*, Vol. 43, 1981, pp. 357–372.

[14]Yee, H. C., "Construction of Explicit and Implicit Symmetric TVD Schemes and Their Applications," *Journal of Computational Physics*, Vol. 68, 1987, pp. 151–179.

[15]Blottner, F. C., Johnson, M., and Ellis, M., "Chemically Reacting Viscous Flow Program for Multi-Component Gas Mixtures," Sandia Labs., SC-RR-70-754, Albuquerque, NM, 1971.

[16]Wilke, C. R., "A Viscosity Equation for Gas Mixtures," *Journal of Chemical Physics*, Vol. 18, No. 4, 1950, pp. 517–519.

[17]Gupta, R. N., Yos, J. M., Thompson, R. A., and Lee, K., "A Review of Reaction Rates and Thermodynamic and Transport Properties for an 11-Species Air Model for Chemical and Thermal Nonequilibrium Calculations to 30,000 K," NASA RP 1232, 1990.

[18]Lee, J. H., "Basic Governing Equations for the Flight Regimes of Aeroassisted Orbital Transfer Vehicles," *Thermal Design of Aeroassisted Orbital Transfer Vehicles*, edited by H. F. Nelson, Vol. 96, Progress in Astronautics and Aeronautics, AIAA, New York, 1985, pp. 3–53.

[19]Dunn, M. C., and Kang, S. W., "Theoretical and Experimental Studies of Re-Entry Plasmas," NASA TR CR-2232, 1973.

[20]Park, C., *Non-Equilibrium Aerothermodynamics*, 1st ed., Wiley, New York, 1990, Chap. 4.

[21]Vincenti, W. C., and Kruger, C. H., *Introduction to Physical Gas Dynamics*, 2nd ed., Krieger, Malabar, FL, 1965, Chap. 7.

[22]Millikan, R. C., and White, D. R., "Systematic of Vibrational Relaxation," *Journal of Chemical Physics*, Vol. 39, No. 12, 1963, pp. 3209–3213.

[23]Scott, C. D., "Wall Catalytic Recombination and Boundary Conditions in Nonequilibrium Hypersonic Flows—with Applications," *Advances in Hypersonics*, edited by J. J. Bertin, J. Periaux, and J. Ballmann, Vol. 2, Birkhäuser, Boston, 1992, pp. 176–249.

[24]Bruno, C., "Real Gas Effects," *Hypersonic*, edited by J. Periaux, J. J. Bertin, and R. Glowinski, Birkhäuser, Boston, 1989, pp. 303–354.

[25]Halpern, B., and Rosner, D. E., "Chemical Energy Accommodation at Catalyst Surfaces," *Journal of the Chemical Society, Faraday Transactions I*, Vol. 74, 1978, pp. 1883–1912.

[26]Doremus, R. H., *Glass Science*, 1st ed., Wiley, New York, 1978, Chap. 3.

[27]Coffee, T. P., and Heimerl, J. M., "Transport Algorithms for Premixed Laminar Steady State Flames," U.S. Army Ballistic Research Lab., ARBRL-TR-02302, Aberdeen Proving Ground, MD, March 1981.

[28]Hirschfelder, J. O., Curtiss, C. F., and Bird, R. B., *Molecular Theory of Gases and Liquids*, 2nd ed., Wiley, New York, 1964, Chap. 7.

[29]Anderson, J. D., Jr., *Hypersonic and High Temperature Gas Dynamics*, 1st ed., McGraw–Hill, New York, 1989, Chap. 17.

[30]Grumet, A. A., Anderson, J. D., and Lewis, M. J., "A Numerical Study of Shock Wave/Boundary Layer Interaction in Non-Equilibrium Chemically Reacting Air: the Effects of Catalytic Walls," AIAA Paper 91-0245, Jan. 1991.

[31]Gupta, R. N., "Stagnation Flowfield Analysis for an Aeroassisted Vehicle," *Journal of Spacecraft and Rockets*, Vol. 30, No. 1, 1993, pp. 14–21.

[32]Kolodziej, P., and Stewart, D. A., "Nitrogen Recombination on High-Temperature Reusable Surface Insulation and the Analysis of its Effects on Surface Catalysis," AIAA Paper 87-1637, June 1987.

I. D. Boyd
Associate Editor